

12-2000

Photo-induced isotopic fractionation

Charles E. Miller
Haverford College

Yuk L. Yung

Follow this and additional works at: http://scholarship.haverford.edu/chemistry_facpubs

Repository Citation

C.E. Miller, Y.L. Yung, "Photo-induced isotopic fractionation", *J. Geophys. Res.—Atmospheres* 105, 29039-29051 (2000).

This Journal Article is brought to you for free and open access by the Chemistry at Haverford Scholarship. It has been accepted for inclusion in Faculty Publications by an authorized administrator of Haverford Scholarship. For more information, please contact nmedeiro@haverford.edu.

Photo-induced isotopic fractionation

Charles E. Miller

Department of Chemistry, Haverford College, Haverford, Pennsylvania

Yuk L. Yung

Division of Geological and Planetary Sciences, California Institute of Technology, Pasadena, California

Abstract. This paper presents a systematic method for the analysis of photo-induced isotopic fractionation. The physical basis for this fractionation mechanism centers on the fact that isotopic substitution alters the energy levels, molecular symmetries, spin statistical weights and other fundamental molecular properties, producing spectroscopic signatures distinguishable from that of the parent isotopomer. These mass-dependent physical properties are identical to those invoked by Urey to explain stable isotope fractionation in chemical systems subject to thermodynamic equilibrium. Photo-induced isotopic fractionation is a completely general phenomenon and should be observable in virtually all gas phase photochemical systems. Water photo-induced isotopic fractionation has been examined in detail using experimental and theoretical data. These results illustrate the salient features of this fractionation mechanism for molecules possessing continuous UV absorption spectra and unit photodissociation quantum yields. Using the photo-induced isotopic fractionation methodology in conjunction with standard photochemical models, we predict substantial deuterium enrichment of water vapor in the planetary atmospheres of Earth and Mars.

1. Introduction

Stable isotope fractionation for molecules composed of light elements has been known since the 1930s. Urey first recognized that the mass dependence of vibrational and, to a lesser extent, rotational frequencies would alter the quantum mechanical partition functions of isotopomers to produce measurable differences in chemical equilibria, chemical reaction rates, and isotopic fractionation [Urey, 1947]. Urey's seminal work demonstrated that the physical basis of isotopic fractionation was "well correlated with the energy states of molecules as secured from spectral data by the use of statistical mechanics" [Urey, 1947, p. 563]. Thus Urey defined a systematic method for the evaluation of isotopic fractionation in systems that achieve thermodynamic equilibrium. The first applications of this theory concentrated on isotopic fractionation in geological and astrophysical processes. Subsequent work has used improved spectroscopic constants used to calculate the partition functions and fractionation factors [Richet *et al.*, 1977], but the conceptual mechanism for stable isotope fractionation has remained relatively unchanged [Kaye, 1987; Richet *et al.*, 1977].

A number of groups have recently achieved the technical expertise necessary to measure isotopic fractionation of the terrestrial atmospheric trace gases O₃ [Johnston and Thiemens, 1997; Mauersberger, 1987], CO₂ [Brenninkmeijer *et al.*, 1995], CO [Brenninkmeijer *et al.*, 1995; Huff and Thiemens, 1998; Rockmann *et al.*, 1999], CH₄ [Brenninkmeijer *et al.*, 1995; Irtion *et al.*, 1996], and N₂O [Cliff *et al.*, 1999; Cliff and Thiemens, 1997; Kim and Craig, 1993; Rahn and Wahlen, 1997; Yoshida and Matsuo, 1983] with uncertainties approaching 0.1 per mil. Modeling isotopic fractionation measurements of this accuracy

challenges the most basic understanding of global biogeochemical cycles. Data sets that combine atmospheric mixing ratios and isotopic fractionation have sufficient information content to constrain global budgets as well as quantify individual trace gas sources and sinks [Johnston and Thiemens, 1997]. Several groups have also inferred the composition of the paleoatmosphere from the isotopic fractionation found in ice cores [Petit *et al.*, 1999].

The last 30 years have also witnessed tremendous progress in the measurement of isotopic fractionation in the atmospheres of Venus, Mars, Jupiter, Saturn, Uranus, Neptune, and Titan. Many of these studies have focused on the determination of the D/H ratio since this quantity is a sensitive measure of an atmosphere's evolutionary history [Debergh, 1993; Frost *et al.*, 1982; Geiss and Reeves, 1981; Kaye, 1987; Lecluse and Robert, 1994; Owen, 1992; Owen *et al.*, 1986; Thiemens, 1999; Vidal-Madjar *et al.*, 1998; Yung and Dissly, 1992; Yung and Kass, 1998]. Figure 1 presents an overview of the D/H ratios observed in the solar system and in interstellar molecular clouds [Owen, 1992; Vidal-Madjar *et al.*, 1998; Yung and Dissly, 1992]. Of particular interest to the present study are the water vapor measurements in the atmospheres of Mars [Krasnopolsky *et al.*, 1997; Owen *et al.*, 1988], Venus [Encrenaz *et al.*, 1995; Encrenaz *et al.*, 1991], in the stratospheres of the giant planets [Atreya *et al.*, 1999; Encrenaz *et al.*, 1999], and in comets [Blake *et al.*, 1999; Eberhardt *et al.*, 1995]. The interpretation for the observed D/H fractionation pattern has been presented by Yung and Dissly [1992]. Here we emphasize the point that the large deuterium enrichments in the atmospheres of Mars and Venus are believed to be the result of photolytic and kinetic processes.

A key feature of planetary atmospheres is that they are dominated by photochemical processes and do not achieve thermodynamic equilibrium [Kaye, 1987; Kaye, 1992]. Therefore Urey's theory is inadequate to describe the isotopic fractionation observed in these systems. We address this deficiency by presenting the theory of photo-induced isotopic

Copyright 2000 by the American Geophysical Union

Paper number 2000JD900388
0148-0227/00/2000JD900388\$09 00

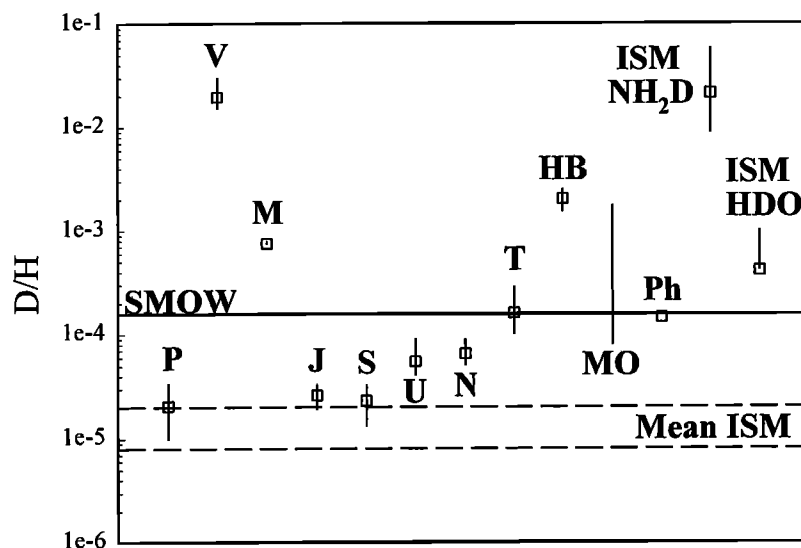


Figure 1. D/H ratios in the solar system and interstellar molecular clouds. The uncertainty and range of variability are indicated by error bars. SMOW, Standard Mean Ocean Water; Mean ISM, Mean Interstellar Medium; P, Protosolar; V, Venus; M, Mars; J, Jupiter; S, Saturn; U, Uranus; N, Neptune; T, Titan; HB, Comet Hale-Bopp; MO, Meteoritic Organics; Ph, Phyllosilicates; ISM NH₂D, Interstellar Medium NH₂D; ISM HDO, Interstellar Medium HDO. Figure after *Yung and Dissly* [1992], with updates. Read 1e-1 as 1×10^{-1} .

fractionation effects (PHIFE), a framework for the systematic evaluation of photochemical isotopic fractionation. We demonstrate that PHIFE is a completely general phenomenon and has the same physical basis as Urey's thermodynamic equilibrium theory of isotopic fractionation. PHIFE should be observable in any photochemically driven planetary atmosphere and may be applied to virtually any parent molecule and its isotopomers. The PHIFE theory explains the isotopic fractionation of different isotopomers regardless of substitution position or the mass of the substituted isotope. PHIFE should be especially important in species for which photodissociation is the dominant destruction mechanism. The PHIFE theory was originally developed to explain the simultaneous enhancement of $\delta^{15}\text{N}$, $\delta^{17}\text{O}$, and $\delta^{18}\text{O}$ signatures in stratospheric N₂O [Miller and Yung, 2000; Yung and Miller, 1997]. It became apparent that PHIFE applied to many different chemical species and was equally valid for modeling the atmospheric photochemistry of the terrestrial planets, the giant planets, satellites, interstellar clouds, etc.

This paper investigates the photo-induced isotopic fractionation of water in the atmospheres of Earth and Mars. The wealth of experimental and theoretical data on water photodissociation also enables us to examine several methods for evaluating PHIFE. The remainder of the paper is organized as follows: Section 2 describes the physical basis for photo-induced isotopic fractionation. Section 3 contains a detailed application of these principles to water photodissociation. Modeling results of water PHIFE in the atmospheres of Earth and Mars are presented in section 4. We conclude with some general remarks on photo-induced isotopic fractionation in section 5.

2. Physical Basis of Photo-Induced Isotopic Fractionation

The principle underlying photo-induced isotopic fractionation is that every isotopomer has a unique spectroscopic signature. This is a direct result of the mass-dependent nature of the quantum mechanical formulae governing molecular energy

levels. Urey [1947] recognized the unique spectral properties of different isotopomers and incorporated this information into his thermodynamic equilibrium theory of isotopic fractionation. The isotopic dependence of a molecular spectrum is readily apparent for rotational or vibrational transitions where the transition frequencies are strongly dependent on the reduced mass of the molecule. Isotopic differences become subtler in electronic absorption spectra since the dependence on the molecular reduced mass is generally much smaller. However, isotopic substitution will cause changes in the molecular symmetry group and the nuclear spin statistics, making the electronic absorption spectra of different isotopomers distinguishable. Therefore PHIFE models treat the photodynamics of each isotopomer independently. The principles of molecular photodissociation used to develop the PHIFE theory are well known [Okabe, 1978; Schinke, 1993; Yung and DeMore, 1999] and the interested reader is directed to these comprehensive texts for more details.

This paper develops the theory of photo-induced isotopic fractionation for molecules with continuous UV absorption spectra and unit photodissociation probability; PHIFE in systems exhibiting predissociation, resolved vibronic structure, or competition between dissociation and radiative decay will be addressed in a future report [C. E. Miller and Y. L. Yung, manuscript in preparation, 2000]. Given that molecule X and its isotopomer X' have unique electronic absorption spectra, it follows that the photodissociation rates for different isotopomers are mass-dependent since

$$J(E) = \sigma(E)I(E) \quad (1)$$

$$J'(E) = \sigma'(E)I(E), \quad (2)$$

where $J(E)$ is the photodissociation rate for photon energy $E = h\nu$, $\sigma(E)$ is the absorption cross section, and $I(E)$ is the photon flux rate. The isotopic enrichment due to an irreversible sink such as photodissociation is described by the Rayleigh distillation equation [Rahn et al., 1998]

$$\delta(E) = \delta_0 + \varepsilon(E) \text{Ln}(f), \quad (3)$$

where $\delta(E)$ is the final fractionation due to photolysis at photon energy $E = h\nu$, δ_0 is the initial sample fractionation, f is the fraction of molecules remaining from the original sample and $\varepsilon(E)$ is a loss factor which may be reexpressed in terms of the absorption cross sections to yield

$$\delta(E) = \delta_0 + 1000 \left(\frac{\sigma'(E)}{\sigma(E)} - 1 \right) \text{Ln}(f) \quad (4)$$

The quantity $\delta(E)$ is expressed in units of per mil. Equation (4) shows that the mass dependence in photo-induced isotopic fractionation arises as a natural consequence of isotopomers having distinguishable spectra. Since the measurement of isotopic fractionation in an atmospheric sample represents contributions from all possible photon energies, it is more correctly calculated from the total integrated photodissociation rate

$$\delta = \delta_0 + 1000 \left(\frac{J'}{J} - 1 \right) \text{Ln}(f), \quad (5)$$

where

$$\frac{J'}{J} = \frac{\int J'(E) dE}{\int J(E) dE} = \frac{\int \sigma'(E) I(E) dE}{\int \sigma(E) I(E) dE}. \quad (6)$$

If photodissociation is a significant sink for the molecule under consideration, then (5) predicts the degree of isotopic fractionation produced during photolysis. One describes the effective photo-induced isotopic enrichment with the function $-\varepsilon(E)$ since $0 \leq f \leq 1$ which means that the $\text{Ln}(f)$ contribution to (3) will always be negative. A value of $-\varepsilon(E) > 0$ indicates enrichment of the isotopomer under consideration while $-\varepsilon(E) < 0$ indicates depletion.

Ideally, the photochemical modeling of PHIFE entails selecting a molecule to investigate, scaling the abundance of each isotopomer to the appropriate initial value, providing experimentally measured UV absorption cross sections for each isotopomer and then executing the model run. The model runs normally in all other ways. The output provides a clear picture of the isotopic fractionation induced by photochemistry. It is often the case that $\sigma'(E)$ the experimental UV absorption spectrum for the isotopomer X' has not been measured but that $\sigma(E)$ is known. One may approximate $\sigma'(E)$ based on the experimental spectrum $\sigma(E)$ and the relative zero point energies (ZPE) of X and X' . This ZPE-shift model [Miller and Yung, 2000; Yung and Miller, 1997] assumes a simple reflection principle treatment of the absorption process [Schinke, 1993] and the invariance of the molecular potential energy surfaces to isotopic substitution (the Born-Oppenheimer approximation). Given a bound ground state and a dissociative upper state, as in Figure 2, one generates the absorption spectrum $\sigma(E)$ by projecting the ground state wave packet $|\Psi_0\rangle^2$ onto the upper state potential surface and then reflecting this projection onto the energy axis. The Gaussian form of $|\Psi_0\rangle^2$ translates into a $\sigma(E)$ which has a nearly Gaussian contour but is compressed at low energies and elongated at higher energies. If the isotopomer X' has a larger reduced mass than X , then its ZPE will be lower. Since the electronic potential surfaces are the same for both isotopomers, the contours of $|\Psi_0\rangle^2$ and $\sigma'(E)$ will be nearly identical to $|\Psi_0\rangle^2$ and $\sigma(E)$. However, since the ground state probability density of the heavier isotopomer resides lower in the potential well, its wave function is confined to a smaller area of coordinate space than that of the

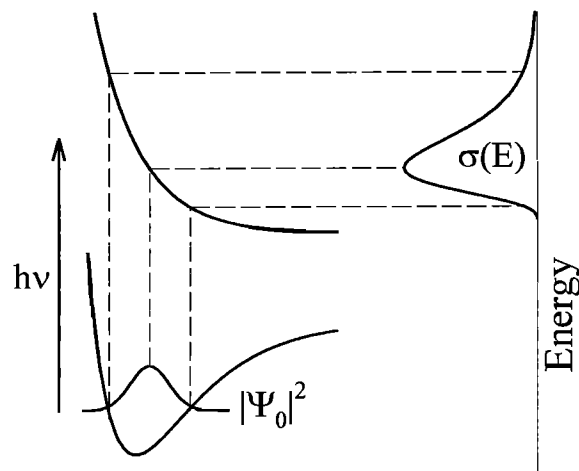


Figure 2. The contour of an electronic absorption spectrum may be viewed as the projection of the ground state molecular wave packet $|\Psi_0\rangle^2$ onto the upper electronic surface and then reflected onto the energy axis. See section 2 for additional details.

parent isotopomer. This results in an absorption spectrum $\sigma'(E)$ that is blue shifted and somewhat narrower than $\sigma(E)$. In cases where the spatial extent of $|\Psi_0\rangle^2$ and $|\Psi_0'\rangle^2$ are negligibly different, the absorption spectrum for the isotopomer X' is defined by the zero point energy difference

$$\sigma'(E + \Delta ZPE) = \sigma(E), \quad (7)$$

where

$$\Delta ZPE = ZPE(X) - ZPE(X'). \quad (8)$$

Using experimentally measured vibrational frequencies for X and X' , the ΔZPE are calculated and $\sigma'(E)$ evaluated. The PHIFE for isotopomer X' are then determined from (4) and (5). One may quickly estimate the relative fractionations for any two isotopomers

$$\frac{\varepsilon_{X'}(E)}{\varepsilon_X(E)} = \frac{\Delta \sigma_{X'}(E)}{\Delta \sigma_X(E)} = \frac{\Delta ZPE_{X'}}{\Delta ZPE_X}, \quad (9)$$

since

$$\Delta \sigma(E) = \frac{d\sigma(E)}{dE} \Delta ZPE. \quad (10)$$

Figure 2 depicts the manner in which isotopic substitution affects the absorption spectra of diatomic molecules. The situation is more complicated for polyatomic molecules where multiple vibrational coordinates must be considered in both the upper and lower electronic states. This requires that the contributions from all vibrational modes be included when calculating ΔZPE for the ground state. The vibrational modes of the upper electronic state will also undergo isotopic shifting, but these shifts may be ignored to a first approximation since molecules undergoing direct photodissociation accelerate along the dissociation coordinate immediately after photoexcitation to the upper electronic state. Thus one may estimate the UV absorption spectrum of a polyatomic molecule with the same basic ZPE-shift methodology developed for diatomic molecules.

For small molecules composed of light atoms, such as water, accurate ab initio calculations of $\sigma(E)$ may be available. The

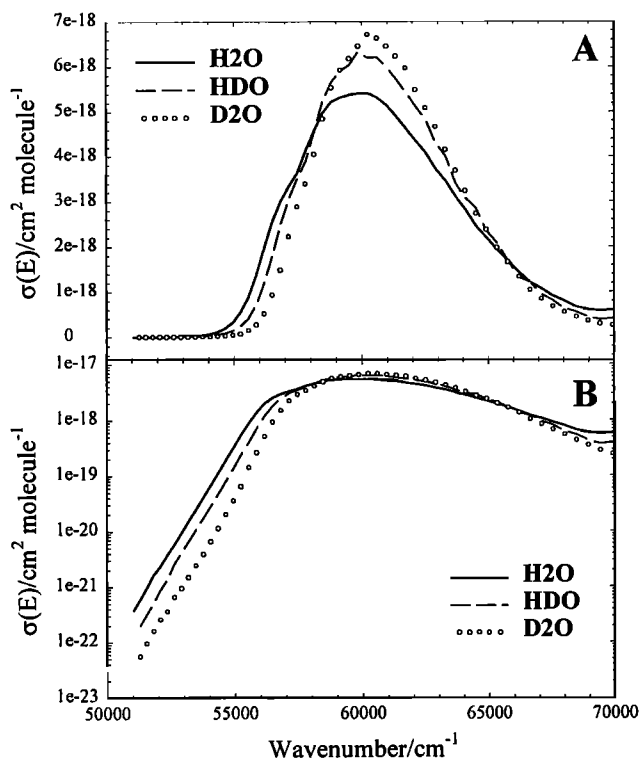


Figure 3. Experimental absorption cross sections for H₂O, HDO, and D₂O [Cheng *et al.*, 1999]. (a) Linear scale. Note the different absorption maxima. (b) Log scale. This plot emphasizes the differences in the cross section values for $E < 57,000 \text{ cm}^{-1}$. Read $7\text{e-}18$ as 7×10^{-18} .

potential energy surfaces involved in the absorption process should be isotopically invariant according to the Born-Oppenheimer approximation, so the calculation of $\sigma'(E)$ for various substituted isotopomers is relatively inexpensive once the global potential surfaces have been calculated. The resulting ab initio absorption cross sections can then be used to generate PHIFE predictions via (4) and (5).

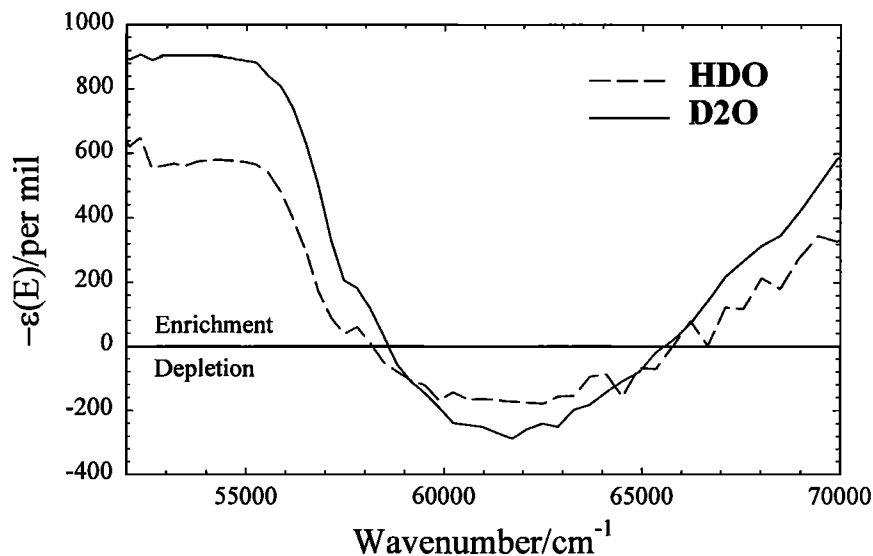


Figure 4. The photo-induced isotopic fractionation functions for HDO and D₂O calculated from the experimental absorption cross sections [Cheng *et al.*, 1999]. Note the exceptionally large fractionation values predicted for photon energies below $55,000 \text{ cm}^{-1}$.

There are caveats associated with PHIFE calculated from ab initio absorption cross sections. Accurate isotopic fractionation determinations will depend on the quality of (1) the global topology of both the ground and excited electronic states, (2) the transition dipole moment function, and (3) the energy separation between the ab initio potentials. Small inaccuracies in any of these components may lead to imprecise results. Additionally, most ab initio absorption calculations are performed only for rotational angular momentum $J_{\text{rot}} = 0$ and neglect all contributions from hot band absorptions. These limitations are investigated in section 3.2.

3. Detailed Example: Water

3.1. PHIFE From Experimental Absorption Spectra

Water is an important photochemical component of the terrestrial and Martian atmospheres, and hydrological cycles play a crucial role in determining the biogeochemistry of each planet. The photodissociation of water via its first absorption band provides an ideal case for which to analyze photo-induced isotopic fractionation effects in detail. This is a benchmark system for the study of direct photodissociation and has been the subject of extensive experimental and theoretical investigation [Schinke, 1993]. Another advantage of using water to demonstrate PHIFE is that deuteration causes large shifts in the absorption spectra and accurate experimental measurements of the absorption cross sections exist for H₂O, HDO, and D₂O at 298 K [Cheng *et al.*, 1999].

The $A \leftarrow X$ electronic transition or A band of the water spectrum is characterized by an absorption continuum extending from 50,000 to 70,000 cm^{-1} . The band displays no discrete vibrational structure, although small vibronic undulations appear as shoulders superimposed on the continuum absorption [Schinke, 1993]. The absorption cross sections of H₂O, HDO, and D₂O [Cheng *et al.*, 1999] are shown in Figure 3. Successive deuteration from H₂O to HDO to D₂O shifts the spectrum to higher energy, in agreement with the predictions of the ZPE-shift model. Deuteration also causes a narrowing in the overall absorption contour and an associated increase in the magnitude of the absorption maximum. The photo-induced isotopic fractionation factors $-\epsilon(E)$ calculated from the experimental

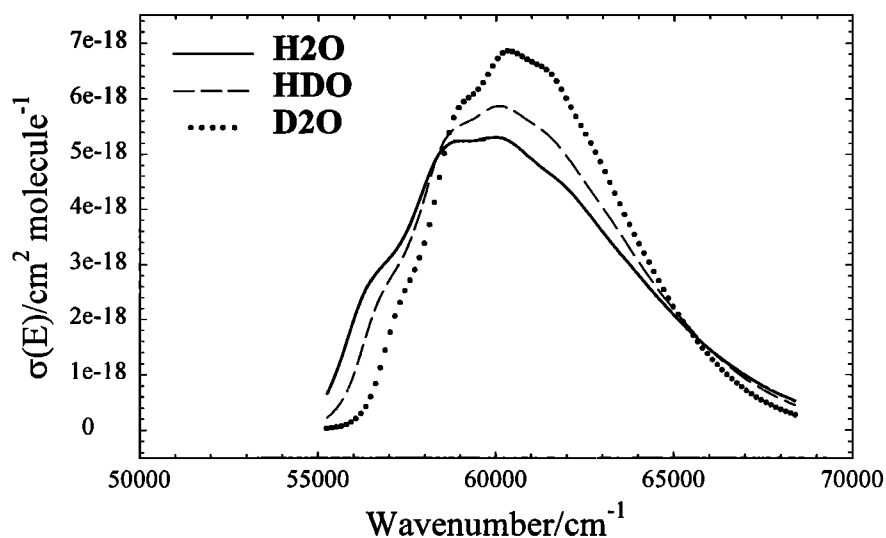


Figure 5. Ab initio absorption cross sections for H₂O, HDO, and D₂O [van Harrevelt and van Hemert, 2000]. Read 7e-18 as 7×10^{-18} .

absorption spectra of H₂O, HDO, and D₂O are shown in Figure 4. The dependence of $-\epsilon(E)$ on isotopomer and photon excitation energy is clearly discerned. For excitation energies below 55,000 cm⁻¹ the $-\epsilon(E)$ factors are essentially constant and very large, reaching 600‰ for HDO and 900‰ for D₂O. The $-\epsilon(E)$ factors decrease with increasing photon excitation energy, becoming negative over the range 58,500 to 66,000 cm⁻¹. Minima in the enrichment factor curves, -180‰ for HDO and -300‰ for D₂O, are observed near 62,000 cm⁻¹. For photon excitation energies above 66,000 cm⁻¹ the enrichment functions again become positive and increase with increasing excitation energy. The overall picture of PHIFE for water thus predicts enrichment of the deuterated isotopomers for photoexcitation below 58,500 cm⁻¹ or above 66,000 cm⁻¹ and depletion of the deuterated species caused by photodissociation in the 58,500 to 66,000 cm⁻¹ region.

The qualitative behavior of the HDO and D₂O photo-induced isotopic fractionation functions does not seem unusual, but the magnitudes of the calculated $-\epsilon(E)$ are 10 to 100 times larger than those typically observed for atmospheric trace gases. Figure 4 illustrates that the $-\epsilon(E)$ are largest at the lowest photon excitation energies. This observation coupled with (1) through (6) suggests that the incident photon flux $I(E)$ will amplify the enrichment of the heavy water isotopomers in planetary atmospheres where a dominant atmospheric constituent effectively absorbs high-energy UV radiation. For example, O₂ and O₃ create an effective atmospheric photodissociation window between 46,000 and 49,000 cm⁻¹ in the terrestrial atmosphere [Yung *et al.*, 1989], while CO₂ eliminates most of the UV flux above 52,000 cm⁻¹ in the Martian atmosphere [Anbar *et al.*, 1993]. Thus water PHIFE in the terrestrial and Martian atmospheres will be dominated by absorption in the low-energy tails of the isotopomer spectra and the deuterium enrichments corresponding to these absorptions (Figure 4).

3.2. Comparison of Different PHIFE Calculations for H₂O, HDO, and D₂O

We now consider water PHIFE determined from experimental, ab initio, and the ZPE-shift absorption spectra. This comparison anticipates the occasions when it will be necessary to estimate PHIFE from an approximation method and to understand the limitations of such an estimate. For example, the water PHIFE

presented in Figure 4 was determined using the experimental absorption cross sections. However, there may be instances when experimental absorption cross sections have not been measured for any/all of the isotopomers of interest. Alternatively, perhaps the spectra are not all of sufficient resolution ($\Delta E \leq 10$ cm⁻¹) and/or accuracy ($\Delta\sigma \leq 0.1 \times 10^{-20}$ cm² molecule⁻¹) to calculate PHIFE with confidence. In these cases the isotopomer absorption cross sections and PHIFE may be obtained from ab initio calculation or the ZPE-shift approximation.

Recently, van Harrevelt and van Hemert [2000] calculated ab initio isotope dependent cross sections for the first absorption band of water; these are shown in Figure 5. The agreement between the experimental and ab initio spectra is very good and demonstrates an excellent theoretical understanding of the water photoabsorption process. The theoretical spectra correctly portray the energy shift and increase in the oscillator strength for HDO and D₂O. The small vibronic shoulders are reproduced as well, although at slightly different energies than in the experimental spectra.

The ZPE-shift approximation was previously used to determine photo-induced isotopic fractionation in stratospheric N₂O [Miller and Yung, 2000; Yung and Miller, 1997]. The estimated absorption cross section shifts for N₂O were only 10 to 55 cm⁻¹, but these small changes were sufficient to induce N₂O fractionation of the order of 10 to 50‰. Subsequent laboratory experiments have verified the photon energy dependence of enrichment functions and our prediction that the position of the ¹⁵N substitution dramatically affects the fractionation [Rahn *et al.*, 1998; Rockmann *et al.*, 2000; Umamoto, 1999]. Deuterium substitutions in water isotopomers lead to ZPE shifts of 615 and 1248 cm⁻¹ for HDO and D₂O, respectively [Partridge and Schwenke, 1997]. These shifts are a factor of 50 larger than those used in the N₂O PHIFE calculations and it is interesting to compare the ZPE-shift approximation to the experimental spectra for HDO and D₂O. The ZPE-shift absorption spectra for HDO and D₂O were calculated from the experimental H₂O cross section by adding 615 and 1248 cm⁻¹, respectively: $\sigma_{\text{HDO}}(E) = \sigma_{\text{H}_2\text{O}}(E+615)$ and $\sigma_{\text{D}_2\text{O}}(E) = \sigma_{\text{H}_2\text{O}}(E+1248)$. The results are shown in Figure 6.

The different PHIFE calculations for HDO and D₂O are compared directly in Figures 7 and 8. The photo-induced isotopic

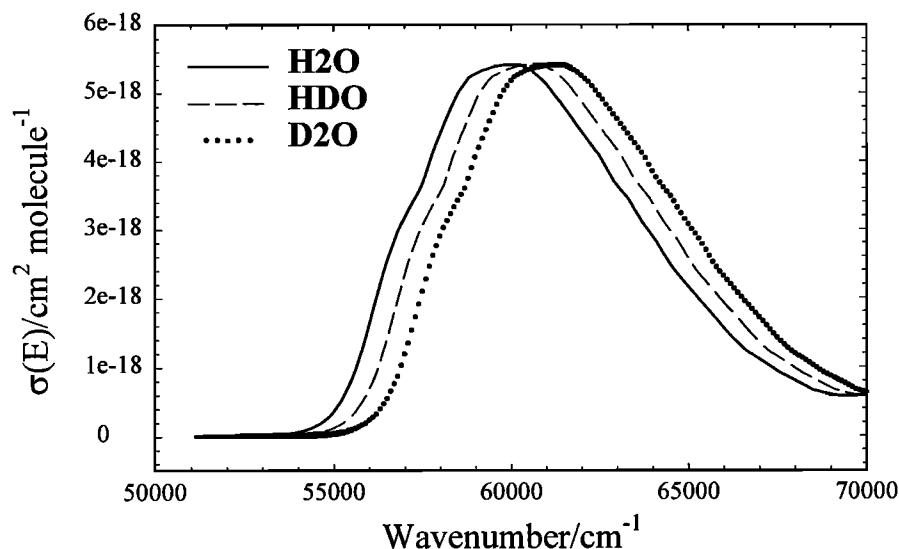


Figure 6. Experimental absorption spectrum for H₂O shown with HDO and D₂O spectra calculated with the ZPE-shift method. Read 6e-18 as 6×10^{-18} .

fractionation functions obtained from the ab initio cross sections reproduce the experimental PHIFE functions quite well over the entire photon energy range. For photon energies less than 55,000 cm⁻¹, the ab initio enrichment functions level off at 700‰ (HDO) and 950‰ (D₂O). The enrichment functions for both deuterated isotopomers decrease with increasing photon energy, passing through zero enrichment near 58,000 cm⁻¹ and reach minima of -100‰ (HDO) and -400‰ (D₂O) near 62,000 cm⁻¹. The enrichment functions then begin to increase and recross the zero enrichment line again near 65,000 cm⁻¹. The major differences between the experimental and ab initio $-\epsilon(E)$ functions are in the magnitudes of the extrema. The ab initio $-\epsilon_{D_2O}(E)$ function overestimates the minimum and maximum enrichments by about 10% while the ab initio $-\epsilon_{HDO}(E)$ function underestimates the minimum enrichment by 30% but overestimates the maximum enrichment by 20%.

The isotopic enrichment functions calculated from the ZPE-shift approximation reproduce the experimental enrichment

functions for photon energies below 57,500 cm⁻¹ remarkably well. The ZPE-shift enrichment functions produce a poor representation of the experimental enrichment functions for photon energies above 57,500 cm⁻¹ since the ZPE-shift method can not account for the increase in the maxima of HDO and D₂O absorption cross sections. The ZPE-shift calculations reproduce the limiting behavior of the enrichment functions for low-energy absorptions, generating values of +650‰ for HDO and +900‰ for D₂O. We note that the ZPE-shift $-\epsilon(E)$ functions reproduce the experimental results better than the ab initio $-\epsilon(E)$ functions for photon energies below 53,000 cm⁻¹. Absorption in the low-energy tail of the water spectrum will be especially important in planetary atmospheres where water is a trace gas and a dominant atmospheric component effectively absorbs higher energy UV radiation.

No experimental UV absorption spectra have been reported for the heavy oxygen isotopomers H₂¹⁷O and H₂¹⁸O, but one may estimate the PHIFE for these isotopomers using the data in Table

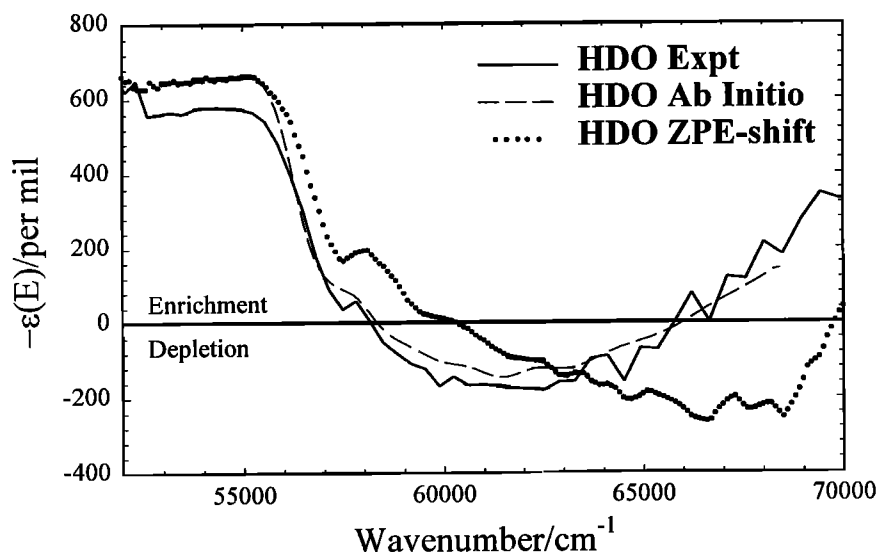


Figure 7. A comparison of the HDO photo-induced isotopic fractionation functions calculated from the experimental, ab initio, and ZPE-shift absorption cross sections.

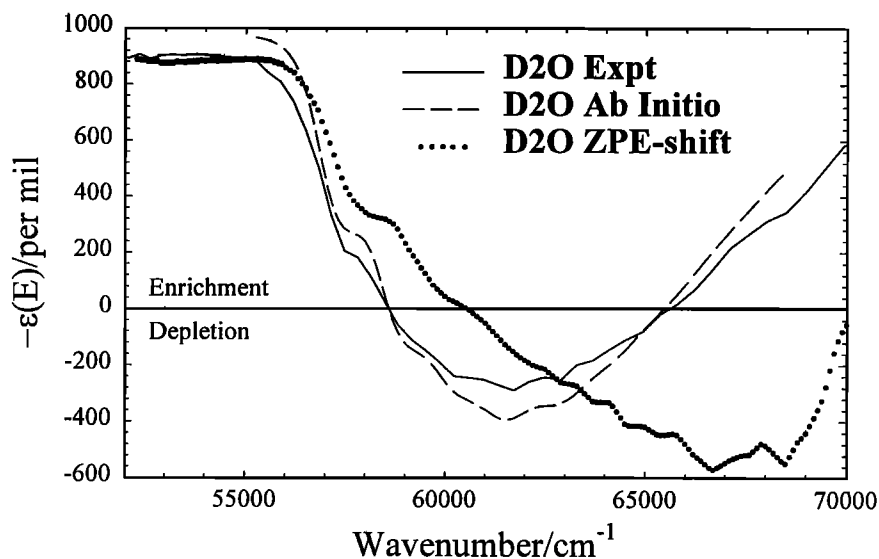


Figure 8. A comparison of the D₂O photo-induced isotopic fractionation functions calculated from the experimental, ab initio, and ZPE-shift absorption cross sections.

1. The zero point energy shifts, 7.92 cm⁻¹ for H₂¹⁷O and 14.98 cm⁻¹ for H₂¹⁸O, are roughly 2 orders of magnitude smaller than the ΔZPE values for the deuterated isotopomers, thus (9) predicts that the PHIFE factors will be a factor of 100 smaller. This is shown in Figure 9. The calculated H₂¹⁷O and H₂¹⁸O fractionations range from 10 to 50‰ for photon energies below 55,000 cm⁻¹. The correct behavior of the fractionation function above 55,000 cm⁻¹ is uncertain, but the values are probably very close to zero. It would be very interesting to have experimental measurements of the PHIFE for H₂¹⁷O and H₂¹⁸O since oxygen isotopic substitution produces such a drastically different fractionation than deuterium substitution.

3.3. Extrapolation of the Water Absorption Cross Sections

An accurate assessment of water PHIFE in the atmospheres of Earth and Mars requires knowledge of the isotopomer absorption cross sections in the 45,000 – 50,000 cm⁻¹ window. The experimental cross sections reported by *Cheng et al.* [1999] do not extend into this region; however, Figure 3b shows that the cross sections below 53,000 cm⁻¹ are small and decreasing exponentially with decreasing photon energy. Using the experimental data for all energies less than 55,000 cm⁻¹, we have extrapolated the experimental data with a linear least squares fit

of log₁₀[σ(*E*)] versus *E* for each isotopomer. The extrapolated cross sections were truncated at a lower limit of 46,500 cm⁻¹. Below this value, absorption is insignificant and Rayleigh scattering becomes the dominant photoprocess. The results of the least squares fits are given in Table 2 and Figure 10.

The extrapolations predict that the absorption cross sections for H₂O, HDO, and D₂O drop below of 1.0 × 10⁻²⁴ cm² molecule⁻¹ at photon energies of 47,391, 48,263 and 48,896 cm⁻¹, respectively. A comparison of the cross sections at this limit yields spectral shifts of 872 and 1605 cm⁻¹ for HDO and D₂O relative to H₂O. These results are in reasonable agreement with the ΔZPE values of 615 and 1248 cm⁻¹ reported in Table 1 and suggest that the ZPE-shift PHIFE calculation provides a reliable reproduction of the experimental photo-induced fractionation function below 55,000 cm⁻¹.

3.4. Summary of the PHIFE Methodology

The principles of photo-induced isotopic fractionation have been presented with a detailed analysis of water photodissociation via the first absorption band. We emphasize that isotope-dependent experimental absorption cross sections should be used in PHIFE calculations to ensure optimal accuracy. Absent experimental data for all of the desired isotopomers, one may approximate PHIFE reasonably well with ab initio calculations or absorption spectra calculated from the ZPE-shift method. For water the ab initio absorption spectra provided a very good global representation of the isotope enrichment functions, although the agreement was not as good in the low-

Table 1. Zero Point Energies (ZPE) and Zero Point Energy Differences (ΔZPE) for Various Water Isotopomers^a

Isotopomer	ZPE cm ⁻¹	ΔZPE cm ⁻¹
H ₂ ¹⁶ O	4638.39	0.00
H ₂ ¹⁷ O	4630.47	7.92
H ₂ ¹⁸ O	4623.41	14.98
HD ¹⁶ O	4023.01	615.38
HD ¹⁷ O	4013.67	624.72
HD ¹⁸ O	4005.34	633.05
D ₂ ¹⁶ O	3390.26	1248.13
D ₂ ¹⁷ O	3379.40	1258.99
D ₂ ¹⁸ O	3369.70	1268.69

^aZPE data calculated by D. Schwenke from the results of *Partridge and Schwenke* [1997].

Table 2. Extrapolated Water Isotopomer Absorption Cross Section Parameters^a

Fit Parameter	H ₂ O	HDO	D ₂ O
m	-59.268	-61.163	-61.499
b	7.419	7.700	7.653
r ²	0.9998	0.9994	0.9977
σ(<i>E</i>) = 1 × 10 ⁻²⁴			
intercept cm ⁻¹	47,391	48,263	48,996

^aParameters derived from a linear least squares fit to log₁₀[σ(*E*)] versus *E* from the absorption cross section data of *Cheng et al.* [1999] for *E* < 55,000 cm⁻¹.

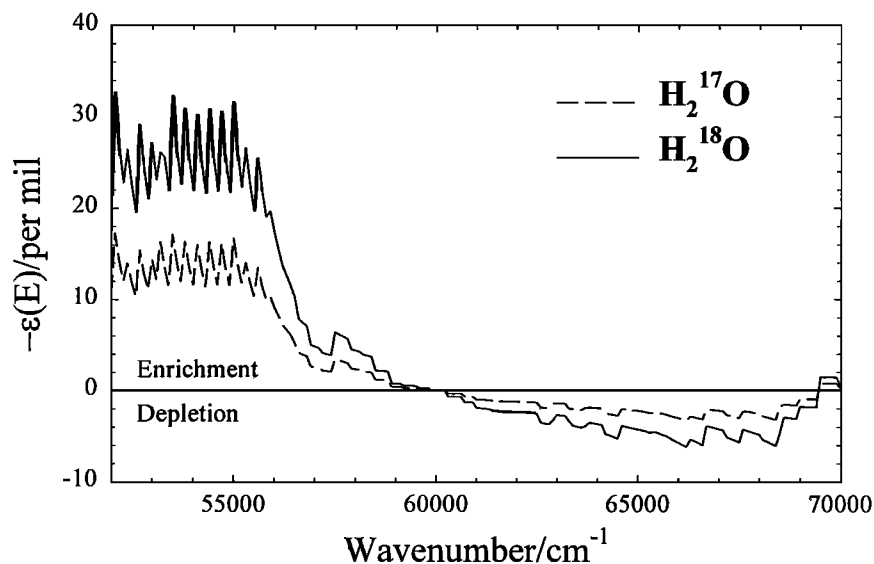


Figure 9. H_2^{17}O and H_2^{18}O photo-induced isotopic fractionation functions calculated using the ZPE-shift method.

energy region where the absorption cross sections are small. The ZPE-shift method produced enrichment functions that agreed well with the experimental $-\epsilon(E)$ for energies below $55,000\text{ cm}^{-1}$ but failed to yield the correct behavior at higher photon energies.

There has been very limited exploration of PHIFE in water isotopomers [Plusquellic *et al.*, 1997; Shafer *et al.*, 1989] despite the large number of water photodissociation experiments that have been performed. Laboratory experiments should be conducted to confirm the predicted enrichment and depletion of HDO and D_2O as a function of photon energy. In anticipation of such experiments, Table 3 provides calculations of water isotopomer PHIFE at some common photodissociation wavelengths. An accurate assessment of water PHIFE in planetary atmospheres requires that measurements of the experimental absorption cross sections for all water isotopomers be extended into the $45,000 - 50,000\text{ cm}^{-1}$ range (see below). An experimental determination of the temperature dependence of the water isotopomer absorption spectra between 150 and 500 K

would also be valuable for many modeling conditions. Finally, it would be interesting to have experimental measurements of the H_2^{17}O and H_2^{18}O absorption spectra and PHIFE since the fractionations for these isotopomers are predicted to be an order of magnitude smaller than the PHIFE associated with deuterated water isotopomers.

4. Photochemical Modeling of Water Photo-Induced Isotopic Fractionation

4.1. Earth

The experimental UV absorption spectra (Figure 2) have been used to evaluate water PHIFE in the terrestrial atmosphere. The calculations were performed with a version of the two-dimensional (2D) photochemical model reported by Allen *et al.* [1984] that employs updated chemical kinetics [DeMore *et al.*, 1997]. Figure 11 displays the photolysis rates calculated for

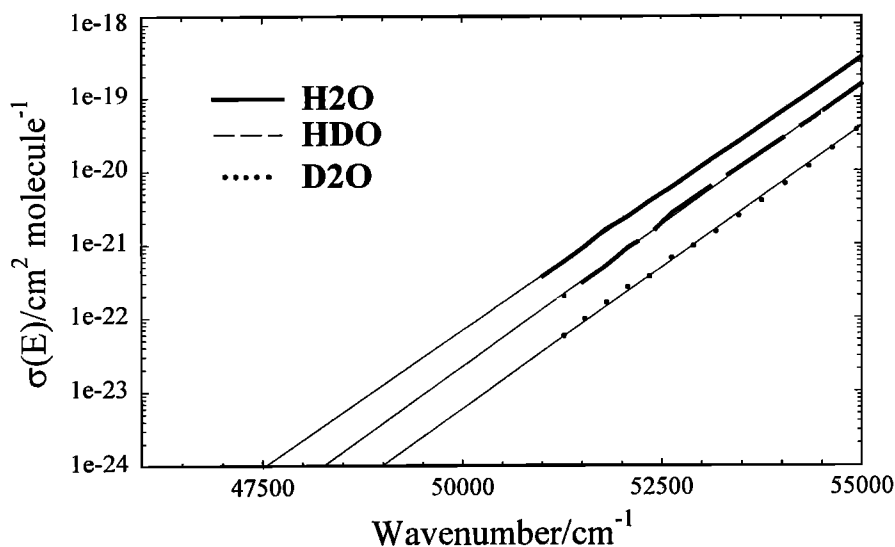


Figure 10. Extrapolated H_2O , HDO, and D_2O absorption cross sections. See section 3.3 and Table 2 for more details.

Table 3. PHIFE for Several Water Isotopomers at Some Common Photodissociation Wavelengths

λ nm	E cm ⁻¹	- $\epsilon(E)$ per mil			
		HD ¹⁶ O	D ₂ ¹⁶ O	H ₂ ¹⁷ O	H ₂ ¹⁸ O
157.5	63,500	-126	-191	-2	-4
184.9	54,100	+578	+902	+16	+30
193.3	51,750	+670	+900	+14	+26
207.0	48,300	+710	+920	N/A	N/A

H₂O, HDO, and D₂O as a function of altitude between 50 and 100 km.

The model predicts three distinct photolysis regions. The lowest altitudes, 50 – 60 km, are characterized by a large disparity in the water isotopomer photolysis rates: $J_{\text{H}_2\text{O}} \sim 2 J_{\text{HDO}}$ and $J_{\text{H}_2\text{O}} \sim 10 J_{\text{D}_2\text{O}}$. The relative ratios of the isotopomer J values remain approximately constant for all altitudes in this range, although all J values increase slowly with increasing altitude. The large differences in photolysis rates and negligible changes in relative photolysis rates are consistent with photolysis in this range dominated by photons with energies less than 55,000 cm⁻¹.

The intermediate altitudes, 60 – 75 km, are characterized by exponential increases in all J values with increasing altitude. It is interesting that $dJ_{\text{D}_2\text{O}}/dz > dJ_{\text{HDO}}/dz > dJ_{\text{H}_2\text{O}}/dz$ throughout this region and that all J -values reach a maximum near 75 km. Additionally, the spread in J values has been dramatically reduced at 75 km: $J_{\text{H}_2\text{O}} < 2 J_{\text{D}_2\text{O}}$. This behavior correlates with the increasing importance of photolysis for energies greater than 55,000 cm⁻¹ for altitudes approaching 75 km.

The upper altitudes, 75 – 100 km, are characterized by a uniform exponential decrease in all J values with increasing altitude. The photolysis rates for all three isotopomers converge to virtually the same values in this region. This suggests that photolysis is dominated by absorptions in the 55,000 – 65,000 cm⁻¹ range, consistent with the larger UV flux expected at higher altitudes.

The column-integrated photolysis rates J_{TOT} are 4.769, 3 500, and 2.781×10^9 cm⁻² s⁻¹ for H₂O, HDO, and D₂O, respectively. These results may be combined with (5) to yield photo-induced isotopic enrichment factors of 266‰ for HDO and 417‰ for

Table 4. Water PHIFE Calculated for the Earth's Upper Atmosphere

Isotopomer	$J_{\text{TOT}} 10^9$ cm ² s ⁻¹	
	Experimental $\sigma(E)$	Extrapolated $\sigma(E)$
H ₂ O	4.769	4.774
HDO	3.500	3.502
D ₂ O	2.781	2 781
- $\epsilon_{\text{TOT}}(\text{HDO})$ ‰	266	266
- $\epsilon_{\text{TOT}}(\text{D}_2\text{O})$ ‰	417	417

D₂O in the total column. A second model run was executed using the extrapolated isotopomer absorption spectra to test the dependence of the water photolysis rates on absorptions below 53,000 cm⁻¹. The results for this case do not differ significantly from those obtained with the unaltered experimental spectra. This conclusion is confirmed by the column-integrated H₂O, HDO, and D₂O photolysis rates, 4.774, 3.502, and 2.781×10^9 cm⁻² s⁻¹ for, respectively, obtained for this simulation. The column-integrated enrichment factors are also identical to those determined in the first simulation. All of the column integrated photolysis rate data is collected in Table 4.

The photo-induced isotopic fractionation derived from the altitude dependent $J_{\text{H}_2\text{O}}$, J_{HDO} , and $J_{\text{D}_2\text{O}}$ is shown in Figure 12. The enrichment functions for HDO and D₂O exhibit three distinct patterns, correlating with the three photolysis regions observed in Figure 11. The enrichment factors remain constant for altitudes in the 50 – 60 km range, with $-\epsilon_{\text{HDO}} \sim 600$ ‰ and $-\epsilon_{\text{D}_2\text{O}} \sim 900$ ‰. These values are the same as those observed at the low-energy limits of the enrichment functions in Figure 4, again indicating that photolysis in this range is due entirely to photon energies less than 55,000 cm⁻¹. The HDO and D₂O enrichment factors decrease rapidly with increasing altitude in the 60 – 75 km range. This is consistent with photolysis contributions from photon energies greater than 55,000 cm⁻¹, but the large enrichments suggest that photolysis below 55,000 cm⁻¹ is still important. The enrichment functions become nearly constant again in the 75 – 100 km range, but they are a factor of 5 smaller than the values in the 50 – 60 km range. This result is interesting in that the model

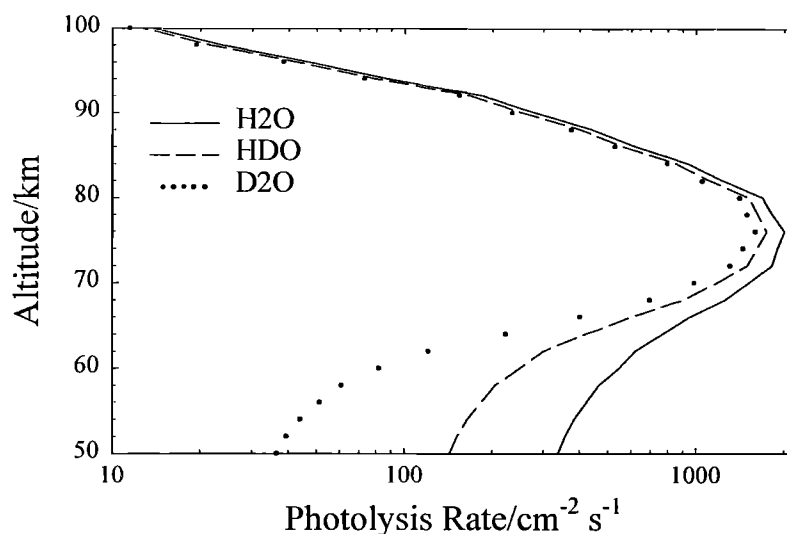


Figure 11. Comparison of the relative photolysis rates for H₂O, HDO, and D₂O in the terrestrial atmosphere calculated using the experimental absorption cross sections [Cheng *et al.*, 1999]. The column-integrated rates are 4.769, 3 500, and 2.781×10^9 cm² s⁻¹, respectively. The model used is based on Allen *et al.* [1984] with the JPL 97-4 kinetics updates [DeMore *et al.*, 1997].

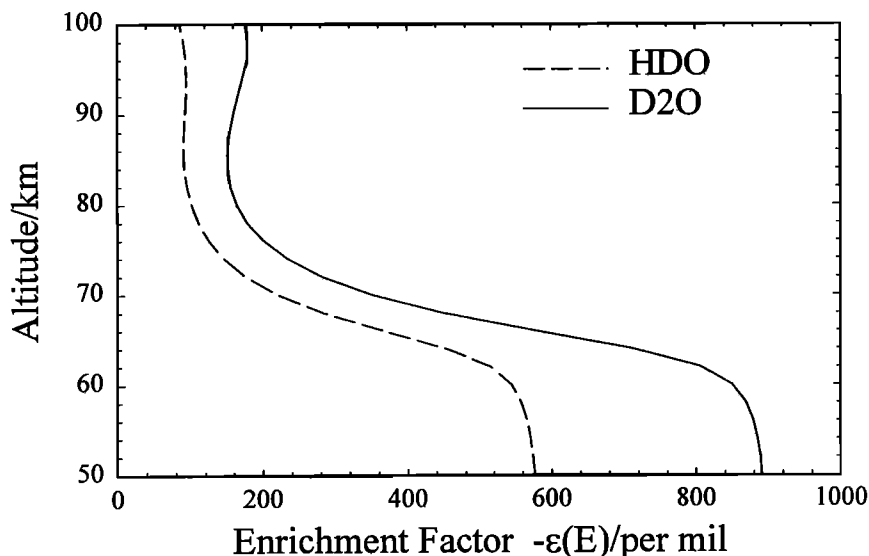


Figure 12. Altitude-dependent HDO and D₂O photo-induced isotopic fractionation predicted for the terrestrial atmosphere. Calculated from the data in Figure 10 (experimental absorption cross sections). The differences between the results for the photolysis rates depicted here and those calculated from the experimental absorption cross sections extrapolated to $46,500 \text{ cm}^{-1}$ (Figure 11) are negligible on the scale of this plot.

predicts that water vapor should be deuterium-enriched at all altitudes, even though the photolysis between 75 and 100 km is dominated by photon energies in the $55,000 - 65,000 \text{ cm}^{-1}$ range.

The results show that the photolysis of HDO in the mesosphere is about 26% less than that for H₂O. Since HDO is the primary source of D to the upper atmosphere, this reduces the efficiency of the escape of D atoms relative H atoms [Yung *et al.*, 1989]. The fractionation of H atoms in the upper atmosphere will be further accentuated by the preferential production of H atoms in HDO photodissociation since the H/D quantum yield ratio ranges from 2 to >100 for photon energies between $50,000$ and $65,000 \text{ cm}^{-1}$ [Schinke, 1993; Shafer *et al.*, 1989]. This mechanism for reducing the escape rate of D atoms must be added to the depletion of HDO across the tropopause due to its preferential condensation relative to H₂O [Moyer *et al.*, 1996]. However, about half of the H₂O in the mesosphere is derived from the oxidation of CH₄, for which no freeze-drying occurs at the tropopause. The consequences of these new results remain to be incorporated into a new model for the evolution of the Earth's atmosphere.

4.2. Mars

A preliminary analysis of photo-induced isotopic fractionation of water in the Martian atmosphere has recently been reported [Cheng *et al.*, 1999; Kass and Yung, 1999]. Water photolysis rates in the Martian atmosphere have been computed using the absorption spectra from Figure 3 and the photochemical model of Nair *et al.* [1994]. The calculated dependence of the H₂O, HDO, and D₂O photolysis rates for altitudes between 0 and 60 km are shown in Figure 13. This figure clearly illustrates that there are major differences between the Martian and terrestrial atmospheres. The most obvious difference is that water photolysis is important all the way to ground level on Mars; this is due to the relative transparency of the Martian atmosphere. The water isotopomer photolysis rates vary by an order of magnitude at the lowest altitude evaluated, as was the case in the terrestrial simulation, but the relative differences in the

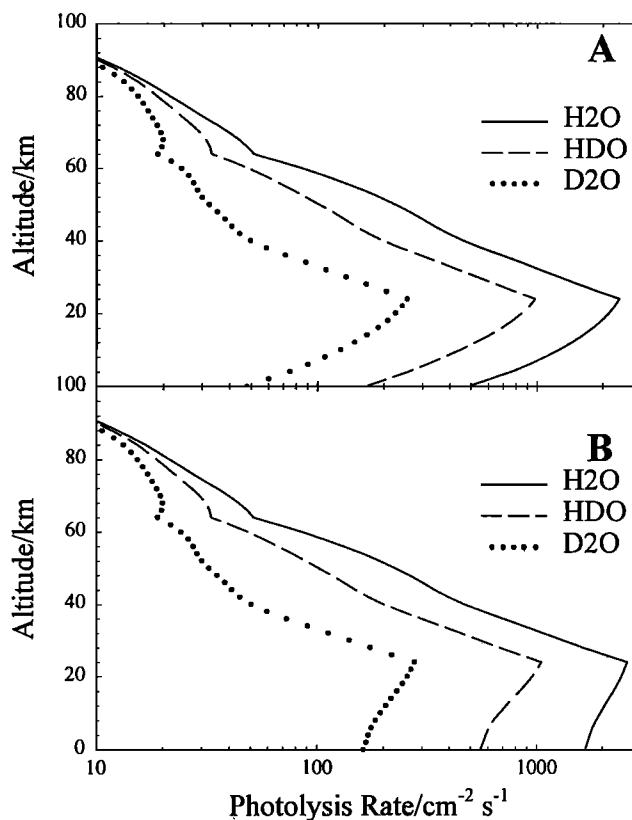


Figure 13. (a) Comparison of the relative photolysis rates for H₂O, HDO and D₂O in the Martian atmosphere calculated using the experimental absorption cross [Cheng *et al.*, 1999]. The column integrated rates are 5.992 , 2.424 and $0.6937 \times 10^9 \text{ cm}^2 \text{ s}^{-1}$, respectively. The model used is based on Nair *et al.* [1994]. (b) Same as Figure 13a, except that the absorption cross sections have been extrapolated to $46,500 \text{ cm}^{-1}$. The column-integrated rates are 7.625 , 2.963 , and $0.8552 \times 10^9 \text{ cm}^2 \text{ s}^{-1}$, respectively.

Table 5. Water PHIFE for Calculated for the Martian Atmosphere

Isotopomer	$J_{TOT} 10^9 \text{ cm}^2 \text{ s}^{-1}$	
	Experimental $\sigma(E)$	Extrapolated $\sigma(E)$
H ₂ O	5.992	7.625
HDO	2.424	2.963
D ₂ O	0.694	0.855
$-\epsilon_{TOT}(\text{HDO}) \text{ ‰}$	595	611
$-\epsilon_{TOT}(\text{D}_2\text{O}) \text{ ‰}$	884	888

isotopomer photolysis rates remain approximately constant in the Martian atmosphere. The photolysis rates do vary as a function of altitude, but the absolute dissociation rates do not converge to a single value for altitudes less than 60 km. The column integrated photolysis rates for the Martian atmosphere, 5.992, 2.424, and $0.6937 \times 10^9 \text{ cm}^2 \text{ s}^{-1}$ for H₂O, HDO, and D₂O, respectively, are significantly more disparate than those calculated for the terrestrial atmosphere. It is interesting to note that the total rates for water photolysis in each atmosphere are of the same order of magnitude. However, $J_{TOT}(\text{H}_2\text{O})$ is 25% larger in the Martian atmosphere than in the terrestrial atmosphere while $J_{TOT}(\text{HDO})$ and $J_{TOT}(\text{D}_2\text{O})$ are 44% and 75% smaller in the Martian atmosphere. This is reflected in the photo-induced isotopic enrichment factors for the Martian atmosphere: 595‰ for HDO and 884‰ for D₂O in the 0–60 km column.

The inclusion of the small, extrapolated components of the water absorption spectra (Figure 10) also has a dramatically different impact on the simulated photolysis rates in the Martian atmosphere. Figure 13b shows that the extrapolated absorption cross sections lead to nearly constant photolysis rates below 20 km for each isotopomer. The differences in the photolysis rates are again separated by a factor of 10 and remain separated by approximately the same amount for all altitudes below 60 km. The column-integrated photolysis rates increase compared to those calculated from the non-extrapolated spectra, but the column integrated photo-induced isotopic enrichment factors are virtually the same, 611‰ for HDO and 888‰ for D₂O. The

column-integrated water photolysis rate data for the Martian atmosphere is collected in Table 5.

Figure 14 displays the altitude-dependent isotopic enrichment factors for HDO and D₂O calculated from the photolysis rates shown in Fig. 13a. The implications of these results for the evolution of Mars have been discussed by *Cheng et al.* [1999] and *Kass and Yung* [1999]. They support the hypothesis that Mars initially possessed a globally averaged water reservoir 50 m deep, but most of this water has escaped. The current globally averaged Martian water reservoir is estimated at 9 m depth and is sequestered in the polar caps. Unlike Earth, fractionation on Mars due to water condensation appears to be less important, at least to first order. This is because the entire Martian atmosphere resembles the terrestrial stratosphere.

5. Concluding Remarks

This paper has presented a systematic method for the evaluation of photo-induced isotopic fractionation effects (PHIFE) in molecules possessing continuous UV absorption spectra and unit photodissociation probability. It was shown that PHIFE arises as a natural consequence of the distinguishable spectral signatures of different isotopomers and that this is necessarily a mass-dependent phenomenon. The PHIFE theory provides an important complement to Urey's theory of isotopic fractionation and enables one to analyze isotopic fractionation patterns in planetary atmospheres where photochemistry produces nonequilibrium conditions. These principles were illustrated with a detailed analysis of water PHIFE in the terrestrial and Martian atmospheres.

Photo-induced isotopic fractionation appears to be a completely general phenomenon and should apply to the photochemistry of all interesting planetary atmospheres. Our treatment of N₂O PHIFE in the terrestrial stratosphere [*Miller and Yung*, 2000; *Yung and Miller*, 1997] prompted experimental studies which verified the wavelength-dependent nature of N₂O isotopic fractionation [*Rahn et al.*, 1998; *Rockmann et al.*, 2000]. The PHIFE theory correctly predicted the magnitude and sign of the isotopic fractionation observed for all N₂O isotopomers in the atmosphere [*Cliff et al.*, 1999; *Cliff and Thieme*, 1997; *Kim and*

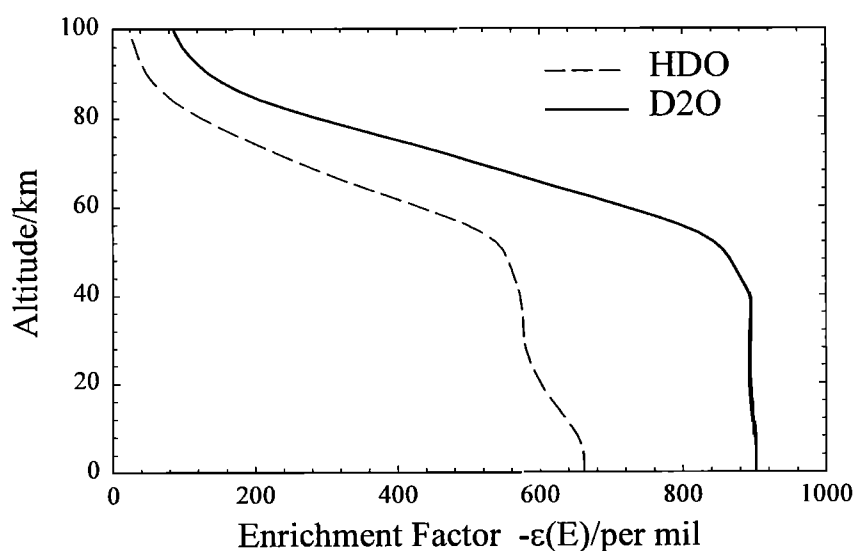


Figure 14. The altitude-dependent HDO and D₂O photo-induced isotopic fractionation predicted for the Martian atmosphere. The differences between the results for the photolysis rates depicted in Figures 13a and 13b are negligible on the scale of this plot.

Craig, 1993; Rahn and Wahlen, 1997; Yoshida and Matsuo, 1983] and an observable difference in the $^{14}\text{N}^{15}\text{N}^{16}\text{O}/^{15}\text{N}^{14}\text{N}^{16}\text{O}$ ratio [Rahn et al., 1998; Rockmann et al., 2000; Umemoto, 1999]. These successes indicate that the theory is fundamentally correct; however, it appears that refinements in the PHIFE simulations are required to achieve complete quantitative agreement with the rapidly increasing database of experimental N_2O measurements. The water PHIFE results from this study provide an interesting perspective on the HO_x cycles of the terrestrial upper atmosphere and on the evolution of the Martian hydrological cycle. Preliminary work suggests that methane, hydrogen chloride, phosphine, and hydrogen sulfide will display PHIFE signatures with magnitudes similar to those of water.

We anticipate that molecules possessing UV absorption spectra with resolved vibronic structure will also produce measurable PHIFE. However, the $\sigma(E)$ functions will be much more complicated than the continuous absorption spectra displayed by molecules undergoing direct dissociation, even for fast predissociation processes that approach 100% dissociation efficiency. Additionally, the isotopic variations of the vibronic absorption features will in general depend on isotopic shifts in both the lower and upper electronic states. The interesting outcome of vibronic spectra PHIFE is that the spectral shifts induced by isotopic substitution often move the absorption features of the isotopomer into regions where the UV flux is higher, especially in the case of an optically thick absorber. This type of behavior was demonstrated for CO isotopomers in interstellar clouds [Cacciani et al., 1998]. Similar effects may contribute to the PHIFE signature of ammonia in the Jovian atmosphere and carbon dioxide in the Martian atmosphere.

The measurement of isotopic fractionation in the trace gas constituents of planetary atmospheres continues to be an active research area. Applications of this data range from the quantification of source and sink terms in global budgets to the characterization of paleoatmospheres. Isotopic fractionation measurements will become increasingly important as the technology for making the measurements improves with the next generation of space-based high-resolution spectrometers (ISO, TESS, FIRST, etc.) and photochemical models. We anticipate that photo-induced isotopic fractionation will prove a valuable addition to the comprehensive understanding of planetary photochemistry.

Acknowledgments. The authors would like to thank Y. P. Lee for the H_2O , HDO, and D_2O absorption cross section data, R. van Harreveld and M. van Hemert for sharing their ab initio absorption cross sections prior to publication, and D. Schwenke for the water isotopomer zero point energies.

References

- Allen, M., J.I. Lunine, and Y.L. Yung, The vertical distribution of ozone in the mesosphere and lower thermosphere, *J. Geophys. Res.*, 89(D3), 4841-4872, 1984.
- Anbar, A.D., M. Allen, and H.A. Nair, Photodissociation in the atmosphere of Mars: Impact of high-resolution, temperature-dependent CO_2 cross-section measurements, *J. Geophys. Res.*, 98(E6), 10,925-10,931, 1993.
- Atreya, S.K., M.H. Wong, T.C. Owen, P.R. Mahaffy, H.B. Niemann, I. de Pater, P. Drossart, and T. Encenaz, A comparison of the atmospheres of Jupiter and Saturn: Deep atmospheric composition, cloud structure, vertical mixing, and origin, *Planet. Space Sci.*, 47, 10-11, 1999.
- Blake, G.A., C. Qi, M.R. Hogerheijde, M.A. Gurwell, and D.O. Muhleman, Sublimation from icy jets as a probe of the interstellar volatile content of comets, *Nature*, 398 (6724), 213-216, 1999.
- Brenninkmeijer, C.A.M., D.C. Lowe, M.R. Manning, R.J. Sparks, and P.F.J. van Velthoven, The ^{13}C , ^{14}C , and ^{18}O isotopic composition of CO , CH_4 , and CO_2 in the higher southern latitudes lower stratosphere, *J. Geophys. Res.*, 100(D12), 26,163-26,172, 1995.
- Cacciani, P., W. Ubachs, P.C. Hinnen, C. Lynga, A. L'Huillier, and C.G. Wahlstrom, Lifetime measurements of the $^1\Pi$, $v=0$ and $v=1$ states of $^{12}\text{C}^{16}\text{O}$, $^{13}\text{C}^{16}\text{O}$, and $^{13}\text{C}^{18}\text{O}$, *Astrophys. J. Lett.*, 499(2), L223-L226, 1998.
- Cheng, B.M., E.P. Chew, C.P. Liu, M. Bahou, Y.P. Lee, Y.L. Yung, and M.F. Gerstell, Photo-induced fractionation of water isotopomers in the Martian atmosphere, *Geophys. Res. Lett.*, 26(24), 3657-3660, 1999.
- Cliff, S.S., and M.H. Thiemens, The O-18/O-16 and O-17/O-16 ratios in atmospheric nitrous oxide: A mass-independent anomaly, *Science*, 278(5344), 1774-1776, 1997.
- Cliff, S.S., C.A.M. Brenninkmeijer, and M.H. Thiemens, First measurement of the $^{18}\text{O}/^{16}\text{O}$ and $^{17}\text{O}/^{16}\text{O}$ ratios in stratospheric nitrous oxide: A mass-independent anomaly, *J. Geophys. Res.*, 104(D13), 16,171-16,175, 1999.
- Debergh, C., The D/H ratio and the evolution of water in the terrestrial planets, *Origins Life Evol. Biosphere*, 23(1), 11-21, 1993.
- DeMore, W.B., S.P. Sander, D.M. Golden, R.F. Hampson, M.J. Kurylo, C.J. Howard, A.R. Ravishankara, C.E. Kolb, and M.J. Molina, Chemical kinetics and photochemical data for use in stratospheric modeling. Eval. 12, NASA Jet Propulsion Lab, Pasadena, Calif., 1997.
- Eberhardt, P., M. Reber, D. Krankowsky, and R.R. Hodges, The D/H and $^{18}\text{O}/^{16}\text{O}$ ratios in water from Comet P/Halley, *Astron. Astrophys.*, 302(1), 301-316, 1995.
- Encenaz, T., E. Lellouch, G. Paubert, and S. Gulkis, First detection of HDO in the atmosphere of Venus at radio wavelengths: An estimate of the H_2O vertical distribution, *Astron. Astrophys.*, 246(1), L63-L66, 1991.
- Encenaz, T., E. Lellouch, J. Cernicharo, G. Paubert, S. Gulkis, and T. Spilker, The thermal profile and water abundance in the Venus mesosphere from H_2O and HDO millimeter observations, *Icarus*, 117(1), 162-172, 1995.
- Encenaz, T., P. Drossart, H. Feuchtgruber, E. Lellouch, B. Bezaud, T. Fouchet, and S.K. Atreya, The atmospheric composition and structure of Jupiter and Saturn from ISO observations: A preliminary review, *Planet. Space Sci.*, 47, 10-11, 1999.
- Frost, R.L., J.E. Beckman, G.D. Watt, G.J. White, and J.P. Phillips, Limits on the D:H mod ratio in the interstellar medium for molecular observations, in *Submillimetre Wave Astronomy*, Cambridge Univ. Press, New York, 1982.
- Geiss, J., and H. Reeves, Deuterium in the solar system, *Astron. Astrophys.*, 93, 1-2, 1981.
- Huff, A.K., and M.H. Thiemens, O-17/O-16 and O-18/O-16 isotope measurements of atmospheric carbon monoxide and its sources, *Geophys. Res. Lett.*, 25(18), 3509-3512, 1998.
- Irion, F.W., et al., Stratospheric observations of CH_3D and HDO from ATMOS infrared solar spectra: Enrichments of deuterium in methane and implications for HD, *Geophys. Res. Lett.*, 23(17), 2381-2384, 1996.
- Johnston, J.C., and M.H. Thiemens, The isotopic composition of tropospheric ozone in three environments, *J. Geophys. Res.*, 102(D21), 25,395-25,404, 1997.
- Kass, D.M., and Y.L. Yung, Water on Mars: Isotopic constraints on exchange between the atmosphere and surface, *Geophys. Res. Lett.*, 26(24), 3653-3656, 1999.
- Kaye, J.A., Mechanisms and observations for isotope fractionation of molecular species in planetary atmospheres, *Rev. Geophys.*, 25(8), 1609-1658, 1987.
- Kaye, J.A., Isotope effects in gas-phase chemical-reactions and photodissociation processes: Overview, *ACS Symp. Ser.*, 502, 1-14, 1992.
- Kim, K.R., and H. Craig, Nitrogen-15 and oxygen-18 characteristics of nitrous oxide: A global perspective, *Science*, 262(5141), 1855-1857, 1993.
- Krasnopolsky, V.A., G.L. Bjoraker, M.J. Mumma, and D.E. Jennings, High-resolution spectroscopy of Mars at 3.7 and 8 μm : A sensitive search for H_2O_2 , H_2CO , HCl, and CH_4 , and detection of HDO, *J. Geophys. Res.*, 102(E3), 6525-6534, 1997.
- Lecluse, C., and F. Robert, Hydrogen isotope exchange reaction rates: Origin of water in the inner solar system, *Geochim. Cosmochim. Acta*, 58(13), 2927-2939, 1994.

- Mauersberger, K., Ozone isotope measurements in the stratosphere, *Geophys. Res. Lett.*, *14*(1), 80-83, 1987.
- Miller, C.E., and Y.L. Yung, Photolysis Induced Isotopic Fractionation Effects in Stratospheric N₂O, *Chemosphere: Global Change Science*, in press, 2000.
- Moyer, E.J., F.W. Irion, Y.L. Yung, and M.R. Gunson, ATMOS stratospheric deuterated water and implications for troposphere-stratosphere transport, *Geophys. Res. Lett.*, *23*(17), 2385-2388, 1996.
- Nair, H., M. Allen, A.D. Anbar, Y.L. Yung, and R.T. Clancy, A photochemical model of the Martian atmosphere, *Icarus*, *111*(1), 124-150, 1994.
- Okabe, H., *Photochemistry of Small Polyatomic Molecules*, 431 pp., John Wiley, New York, 1978.
- Owen, T., Deuterium in the solar-system, *Symp Int Astron. Union*, *150*, 97-101, 1992.
- Owen, T., B.L. Lutz, and C. Debergh, Deuterium in the outer solar-system: Evidence for 2 distinct reservoirs, *Nature*, *320*(6059), 244-246, 1986.
- Owen, T., J.P. Maillard, C. Debergh, and B.L. Lutz, Deuterium on Mars: The abundance of HDO and the value of D/H, *Science*, *240*(4860), 1767-1770, 1988.
- Partridge, H., and D.W. Schwenke, The determination of an accurate isotope dependent potential energy surface for water from extensive ab initio calculations and experimental data, *J. Chem. Phys.*, *106*(11), 4618-4639, 1997.
- Petit, J.R., et al., Climate and atmospheric history of the past 420,000 years from the Vostok ice core, Antarctica, *Nature*, *399*(6735), 429-436, 1999.
- Plusquellic, D.F., O. Votava, and D.J. Nesbitt, Photodissociation dynamics of jet-cooled H₂O and D₂O in the non-Franck-Condon regime: Relative absorption cross sections and product state distributions at 193 nm, *J. Chem. Phys.*, *107*(16), 6123-6135, 1997.
- Rahn, T., and M. Wahlen, Stable isotope enrichment in stratospheric nitrous oxide, *Science*, *278*(5344), 1776-1778, 1997.
- Rahn, T., H. Zhang, M. Wahlen, and G.A. Blake, Stable isotope fractionation during ultraviolet photolysis of N₂O, *Geophys. Res. Lett.*, *25*(24), 4489-4492, 1998.
- Richet, P., Y. Bottinga, and M. Javoy, A review of hydrogen, carbon, nitrogen, oxygen, sulphur and chlorine stable isotope fractionation among gaseous molecules, *Annu. Rev. Earth Planet. Sci.*, *5*, 65-110, 1977.
- Rockmann, T., C.A.M. Brenninkmeijer, P.J. Crutzen, and U. Platt, Short-term variations in the ¹³C/¹²C ratio of CO as a measure of Cl activation during tropospheric ozone depletion events in the Arctic, *J. Geophys. Res.*, *104*(D1), 1691-1697, 1999.
- Rockmann, T., C.A.M. Brenninkmeijer, M. Wollenhaupt, J.N. Crowley, and P.J. Crutzen, Measurement of the isotopic fractionation of (NNO)-N-15-N-14-O-16, (NNO)-N-14-N-15-O-16 and (NNO)-N-14-N-14-O-18 in the UV photolysis of nitrous oxide, *Geophys. Res. Lett.*, *27*(9), 1399-1402, 2000.
- Schinke, R., *Photodissociation Dynamics: Spectroscopy and Fragmentation of Small Polyatomic Molecules*, 417 pp., Cambridge Univ. Press, New York, 1993.
- Shafer, N., S. Satyapal, and R. Bersohn, Isotope effect in the photodissociation of HDO at 157.5 nm, *J. Chem. Phys.*, *90*(11), 6807-6808, 1989.
- Thiemens, M.H., Mass-independent isotope effects in planetary atmospheres and the early solar system, *Science*, *283*(5400), 341-345, 1999.
- Umemoto, H., ¹⁴N/¹⁵N isotope effect in the UV photodissociation of N₂O, *Chem. Phys. Lett.*, *314*(3-4), 267-272, 1999.
- Urey, H.C., The thermodynamic properties of isotopic substances, *J. Chem. Soc.*, 562-581, 1947.
- van Harrevelt, R., and M.C. van Hemert, Photodissociation of water. I. Electronic structure calculations for the excited states, *J. Chem. Phys.*, *112*(13), 5777-5786, 2000.
- Vidal-Madjar, A., R. Ferlet, and M. Lemoine, Deuterium observations in the galaxy, *Space Sci. Rev.*, *84*(1-2), 297-308, 1998.
- Yoshida, N., and S. Matsuo, Nitrogen isotope ratio of atmospheric N₂O as a key to the global cycle of N₂O, *Geochem. J.*, *17*(5), 231-239, 1983.
- Yung, Y.L., and W.B. DeMore, *Photochemistry of Planetary Atmospheres*, 456 pp., Oxford Univ. Press, New York, 1999.
- Yung, Y.L., and R.W. Dills, Deuterium in the solar-system, *ACS Symp. Ser.*, *502*, 369-389, 1992.
- Yung, Y.L., and D.M. Kass, Deuteronomy? A puzzle of deuterium and oxygen on Mars, *Science*, *280*(5369), 1545-1546, 1998.
- Yung, Y.L., and C.E. Miller, Isotopic fractionation of stratospheric nitrous oxide, *Science*, *278*(5344), 1778-1780, 1997.
- Yung, Y.L., J.S. Wen, J.I. Moses, B.M. Landry, M. Allen, and K.J. Hsu, Hydrogen and deuterium loss from the terrestrial atmosphere: A quantitative assessment of nonthermal escape fluxes, *J. Geophys. Res.*, *94*(D12), 14,971-14,989, 1989.
-
- C. E. Miller, Department of Chemistry, Haverford College, Haverford, PA 19041-1392. (cmiller@haverford.edu)
- Y. L. Yung, Mail Stop 150-21, Division of Geological and Planetary Sciences, California Institute of Technology, Pasadena, CA 91125. (yly@mercuri.gps.caltech.edu)

(Received April 17, 2000; revised June 13, 2000, accepted June 23, 2000.)